Inorganic Chemistry
Article

Inorg. Chem. **2009**, *48*, 5725–5735 **5725**
DOI: 10.1021/ic8022369

Water-Free Rare Earth-Prussian Blue Type Analogues: Synthesis, Structure, Computational Analysis, and Magnetic Data of $\{Ln^{III}(DMF)_6Fe^{III}(CN)_6\}_\infty$ (Ln = Rare Earths Excluding Pm)

Duane C. Wilson,[†] Shengming Liu,[†] Xuenian Chen,[†] Edward A. Meyers,[†] Xiaoguang Bao,[†] Andrey V. Prosvirin,*[,‡] Kim R. Dunbar,*[,‡] Christopher M. Hadad,[†] and Sheldon G. Shore*[,†]

[†]*Department of Chemistry, The Ohio State University, Columbus, Ohio, 43210, and* [‡]*Department of Chemistry, Texas A&M University, College Station, Texas 77842-3012*

Received November 20, 2008

Water-free rare earth(III) hexacyanoferrate(III) complexes, $\{Ln(DMF)_6(\mu\text{-}CN)_2Fe(CN)_4\}_\infty$ (DMF = *N,N*-dimethylformamide; Ln = Sm, **1**; Eu, **2**; Gd, **3**; Tb, **4**; Dy, **5**; Ho, **6**; Er, **7**; Tm, **8**; Yb, **9**; Lu, **10**; Y, **11**; La, **12**; Ce, **13**; Pr, **14**; Nd, **15**), were synthesized in dry DMF through the metathesis reactions of $[(18\text{-crown-6})K]_3Fe(CN)_6$ with $LnX_3(DMF)_n$ (X = Cl or NO_3). Anhydrous DMF solutions of $LnX_3(DMF)_n$ were prepared at room temperature from $LnCl_3$ or $LnX_3 \cdot nH_2O$ under a dynamic vacuum. All compounds were characterized by IR, X-ray powder diffraction (except for **10**), and single crystal X-ray diffraction (except for **2**, **7**, **10**). Infrared spectra reveal that a monotonic, linear relationship exists between the ionic radius of the lanthanide and the $\nu_{\mu\text{-CN}}$ stretching frequency of **1**−**10**, **12**−**15** while **11** deviates slightly from the ionic radius relationship. X-ray powder diffraction data are in agreement with powder patterns calculated from single crystal X-ray diffraction results, a useful alternative for bulk sample confirmation when elemental analysis data are difficult to obtain. Eight-coordinate Ln(III) metal centers are observed for all structures. *trans*-cyanide units of $[Fe(CN)_6]^{3-}$ formed isocyanide linkages to Ln(III) resulting in one-dimensional polymeric chains. Structures of compounds **1**−**9** and **11** are isomorphous, crystallizing in the space group *C*2/*c*. Structures of compounds **12**−**15** are also isomorphous, crystallizing in the space group *P*2/*n*. One unique polymeric chain exists in the structures of **1**−**9** and **11** while two unique polymeric chains exist in structures of **12**−**15**. One of the polymeric chains of **12**−**15** is similar to that observed for **1**−**9**, **11** while the other is more distorted and has a shorter Ln-Fe distance. Magnetic susceptibility measurements for compounds **3**−**6**, **8**, **11** were performed on polycrystalline samples of the compounds.

Introduction

Previously, we prepared[1] a number of cyanide bridged lanthanide-transition metal complexes that are extended arrays. Our interest in such complexes is based upon not only the possible discovery of new structural types but also the possibility of preparing useful materials as heterogeneous catalyst precursors. For example, we have shown that cyanide bridged lanthanide-palladium complexes are heterogeneous bimetallic catalyst precursors. When such complexes are loaded onto a silica support and reduced, bimetallic nanospecies are produced for the selective catalytic hydrogenation of phenol to cyclohexanone and the hydrodechlorination of chlorobenzenes to benzene. These particles are more effective catalysts than palladium alone or catalysts prepared by separate impregnation of the metals.[1]

While a significant number of hydrated Ln-Fe$(CN)_6$ complexes have been reported, to our knowledge, the synthesis of anhydrous DMF-Ln-Fe$(CN)_6$ systems have not been reported previously. Anhydrous and hydrated Ln-Fe$(CN)_6$ are potential heterogeneous catalyst precursors for Fischer Tropsch chemistry.[2] It will be of interest to compare activities of catalysts derived from the anhydrous and hydrated Ln-Fe$(CN)_6$ complexes with catalysts derived from separate impregnation of the metals on a silica support.

Perhaps the simplest[3,4] examples of Prussian Blue rare earth analogues are $Ln[Fe(CN)_6] \cdot nH_2O$ (Ln = Y, La, Nd; n = 4), reported by Grant and James[5] in 1917. Prandtl and Mohr[6] reported a procedure to obtain crystals of $Ln[Fe(CN)_6] \cdot nH_2O$ (Ln = La, Pr, Nd, Sm, Gd, Dy, Er, Y). Single crystal X-ray structures were solved for $La[Fe(\mu\text{-}CN)_6] \cdot 5H_2O$ (hexagonal, $P6_3/m$)[7] and $Sm[Fe(\mu\text{-}CN)_6] \cdot 4H_2O$ (orthorhombic, *Cmcm*),[8] three-dimensional extended arrays.

*To whom correspondence should be addressed. E-mail: shore.1@osu.edu.

(1) (a) Shore, S. G.; Ding, E.; Park, C.; Keane, M. A. *Catal. Commun.* **2002**, *3*, 77–84. (b) Shore, S. G.; Ding, E.; Park, C.; Keane, M. A. *J. Mol. Catal. A: Chem.* **2004**, *212*, 291. (c) Jujjuri, S.; Ding, E.; Hommel, E. L.; Shore, S. G.; Keane, M. A. *J. Catal.* **2006**, *239*, 486–500. (d) Jujjuri, S.; Ding, E.; Shore, S. G.; Keane, M. A. *J. Mol. Catal. A: Chem.* **2007**, *272*, 96–107.

(2) Maitlis, P. M. *J. Organomet. Chem.* **2004**, *689*, 4366–4374.
(3) Dunbar, K. R.; Heintz, R. A. *Prog. Inorg. Chem.* **1997**, *45*, 283–391.
(4) Tanase, S.; Reedijk, J. *Coord. Chem. Rev.* **2006**, *250*, 2501–2510.
(5) Grant, A. J.; James, C. *J. Am. Chem. Soc.* **1917**, *39*, 933–937.
(6) Prandtl, W.; Mohr, S. *Z. Anorg. Allgem. Chem.* **1938**, *236*, 243–251.
(7) Bailey, W. E.; Williams, R. J.; Milligan, W. O. *Acta Crystallogr.* **1973**, *B29*, 1365–1368.
(8) (a) Kietaibl, H.; Petter, W. *Helv. Phys. Acta* **1974**, *47*, 425. (b) Petter, W.; Gramlich, V.; Hulliger, F. *J. Solid State Chem.* **1989**, *82*, 161–167.

Published on Web 06/09/2009

The completed series (excluding Pm) consisted of only the hexagonal (Ln = La, Ce, Pr, Nd) and orthorhombic (Ln = all rare earths except La) structure types.[9] Salts that can exhibit both structural types (Ln = Ce, Pr, Nd) crystallize in the orthorhombic system when the reaction is performed at elevated temperatures.

A decade ago, *N,N*-dimethylformamide (DMF) was incorporated as a blocking ligand to generate alternative coordination of $[(\mu\text{-CN})_{6-x}\text{Fe(CN)}_x]^{3-}$ with Ln^{3+}. The resulting structure with space group $P2_1/c$ was reported as $[\text{Ln(DMF)}_4(\text{H}_2\text{O})_m(\mu\text{-CN})\text{Fe(CN)}_5]\cdot n\text{H}_2\text{O}$ (Ln = Sm, $m = 4$, $n = 1$), a discrete molecular compound.[10] This is the only compound of the rare earth series found for which $m = 4$. Single crystal X-ray structures of this type where $m = 3$ and $n = 1$ have been reported for La, Ce,[11] Pr,[12] Nd,[13] Sm,[14] Eu,[15] Gd,[14,16] Dy ($n = 1.25$),[17] Er,[18] Tm ($n = 1.25$),[12] Yb, and Lu;[18] however, analogous structures containing Pm, Tb, Ho, and Y are unknown.

More recently, the compounds $[\text{Sm(DMF)}_2(\text{H}_2\text{O})_3(\mu\text{-CN})_3\text{Fe(CN)}_3]\cdot\text{H}_2\text{O}$, with two-dimensional extended sheets, and $[\text{Sm(DMF)}(\text{H}_2\text{O})_3(\mu\text{-CN})_4\text{Fe(CN)}_2]\cdot\text{H}_2\text{O}$, with two-dimensional extended bilayers, have been synthesized by a ball-milling method that manipulates reagent concentrations.[19] The former compound has bridging cyanide units in a meridional coordination while the latter has non-bridging cyanides in a *cis* coordination. The complex $\text{Sm(DMF)}_4(\text{H}_2\text{O})_2(\mu\text{-CN})_2\text{Fe(CN)}_4\cdot\text{H}_2\text{O}$ was synthesized as a one-dimensional polymeric chain with the bridging cyanides in a *cis* coordination using *tetra-n*-butylammonium hexacyanoferrate(III).[20]

There are a growing number of reports of DMF-H_2O-Ln-Fe(CN)_6 systems with varying amounts of Ln coordinated by DMF (for which the number of DMF units is 0, 1, 2, 4, and 6). Examples of molecular as well as one-, two-, and three-dimensionalities, as well as five unique modes of $[\text{Fe(CN)}_6]^{3-}$ isocyanide coordination, have been reported. The rich structural chemistry of such simple building blocks has yet to be exhausted as more combinations of DMF and H_2O remain unreported for this system. Indeed, the $\text{Ln(DMF)}_6\text{Fe(CN)}_6$ series reported here contain a unique mode of $[\text{Fe(CN)}_6]^{3-}$ isocyanide coordination to Ln(III).

In the present investigation, we report here the syntheses and structures of anhydrous $\text{Ln(DMF)}_6\text{Fe(CN)}_6$ (Ln = Sm, **1**; Eu, **2**; Gd, **3**; Tb, **4**; Dy, **5**; Ho, **6**; Er, **7**; Tm, **8**; Yb, **9**; Lu, **10**; Y, **11**; La, **12**; Ce, **13**; Pr, **14**; Nd, **15**).

Experimental Section

General Procedures. All manipulations were performed in a Vacuum Atmospheres inert atmosphere drybox under dry N_2 or in a standard high-vacuum line unless otherwise stated. Linde brand molecular sieves (type 4 Å) and Celite were dried by heating (ca. 130 °C) under a dynamic vacuum for 12−18 h. DMF was used as received or dried prior to use. DMF was dried by freezing and thawing under a dynamic vacuum and then standing over molecular sieves under a static vacuum for at least 1 day. Dried DMF was filtered through Celite on a frit prior to use. Dry diethyl ether was obtained by distillation from a mixture of anhydrous diethyl ether, sodium metal, and benzophenone. All other reagents were purchased from commercial sources and used as received. All cyanide solutions and products were stored in the dark. Compounds **1**−**15** were synthesized by one of two methods. Experimental procedures for compounds **1** and **4** are presented as examples of the two methods.

$\{\text{Sm(DMF)}_6\text{Fe(CN)}_6\}_\infty$ (1). A mixture of $K_3\text{Fe(CN)}_6$ (0.494 g, 1.50 mmol), 18-crown-6 (1.189 g, 4.499 mmol), and DMF (500 mL, dry) in a 500 mL flask afforded a yellow solution within 1−2 days of stirring (magnetic) and sonication. After filtration through a frit, the clear yellow filtrate was poured into a solution of $SmCl_3$ (0.384 g, 1.50 mmol) in DMF (200 mL, dry). Within 1−2 days at room temperature without disturbance, thin needle-shaped, yellow crystals were produced. The product was collected by vacuum filtration and washed sequentially with dry DMF and dry diethyl ether.

$\{\text{Tb(DMF)}_6\text{Fe(CN)}_6\}_\infty$ (4). A yellow solution was prepared by dissolving $K_3\text{Fe(CN)}_6$ (0.329 g, 1.00 mmol) and 18-crown-6 (0.800 g, 3.03 mmol) in a mixture of H_2O/DMF (10 mL, 1:1) with stirring. The solution was reduced to dryness under a dynamic vacuum. The resulting yellow solid was dissolved in DMF (100 mL) to obtain a yellow solution that was stirred under a dynamic vacuum to afford a yellow powder. DMF (550 mL) was added to dissolve the yellow powder with stirring and placed under a dynamic vacuum to reduce the solvent to 500 mL. The resulting anhydrous solution was filtered through a frit, and stored under N_2. Similarly, a solution of anhydrous $Tb(NO_3)_3$ was prepared by dissolving $Tb(NO_3)_3\cdot 6\text{H}_2\text{O}$ (0.477 g, 1.05 mmol) in DMF (100 mL). Solvent was removed by stirring under a dynamic vacuum at room temperature to afford an anhydrous (confirmed by IR, see Supporting Information) white solid/gel that was re-dissolved in DMF (50 mL). The solvent was removed. The resulting solid/gel was re-dissolved in DMF (125 mL, dry), and the solution was reduced to 100 mL under a dynamic vacuum. The anhydrous $Tb(NO_3)_3$ solution was poured into the anhydrous $[(18\text{-crown-6})\text{K}]_3\text{Fe(CN)}_6$ solution. Within 1−2 days at room temperature without disturbance, thin needle-shaped, yellow crystals were produced. The product was collected by filtration and washed with dry DMF and dry diethyl ether. Product collection and the handling of anhydrous solutions were performed in the drybox. All other manipulations were performed on the bench top.

IR Spectroscopy. IR spectra were recorded from a KBr pellet formed with an Econo-Press Kit (Aldrich). The barrel was sealed under N_2 by clamping an O-ring and a

(9) Hulliger, F.; Landolt, M.; Vetsch, H. *J. Solid State Chem.* **1976**, *18*, 283–291.
(10) Kou, H. -Z.; Yang, G. -M.; Liao, D. -Z.; Cheng, P.; Jiang, Z. -H.; Yan, S. -P.; Huang, X. -Y.; Wang, G. -L. *J. Chem. Crystallogr.* **1998**, *28*, 303–307.
(11) Kautz, J. A.; Mullica, D. F.; Cunningham, B. P.; Combs, R. A.; Farmer, J. M. *J. Mol. Struct.* **2000**, *523*, 175–182.
(12) Figuerola, A.; Diaz, C.; Ribas, C.; Tangoulis, V.; Granell, J.; Lloret, F.; Mahía, J.; Maestro, M. *Inorg. Chem.* **2003**, *42*, 641–649.
(13) Li, G.; Akitsu, T.; Sato, O.; Einaga, Y. *J. Am. Chem. Soc.* **2003**, *125*, 12396–12397.
(14) Li, G.; Akitsu, T.; Sato, O.; Einaga, Y. *J. Coord. Chem.* **2004**, *57*, 855–864.
(15) Li, J. -R.; Cai, L. -Z.; Zou, R. -Q.; Zhou, G. -W.; Guo, G. -C.; Bu, X. -H.; Huang, J. -S. *Acta Crystallogr.* **2002**, *E58*, m686–m687.
(16) Li, J. -R.; Cai, L. -Z.; Guo, G. -C.; Bu, X. -H.; Huang, J. -S. *Acta Crystallogr.* **2004**, *E60*, m259–m261.
(17) Li, J. -R.; Cai, L. -Z.; Zheng, Y.; Guo, G. -C.; Bu, X. -H.; Huang, J. -S. *Wuji Huaxue Xuebao* **2003**, *19*, 91–94.
(18) Mullica, D. F.; Farmer, J. M.; Cunningham, B. P.; Kautz, J. A. *J. Coord. Chem.* **2000**, *49*, 239–250.
(19) Chen, W. -T.; Wang, M. -S.; Cai, L. -Z.; Xu, G.; Akitsu, T.; Akita-Tanaka, M.; Guo, G. C.; Huang, J. S. *Cryst. Growth Des.* **2006**, *6*, 1738–1741.
(20) Ge, C.; Kou, H. -Z.; Ni, Z. -H.; Jiang, Y. -B.; Zhang, L. -F.; Cui, A. -L.; Sato, O. *Chem. Lett.* **2005**, *34*, 1280–1281.

NaCl or KBr window to each side. A Bruker Tensor 27 Fourier-transform spectrometer was used and 32 scans were averaged at 2 cm^{-1} resolution. Bridge stretch occurs at higher frequency than that of terminal stretch. IR $\nu_{(C\equiv N)}$ cm^{-1}: **1**, 2121.16 vs, 2107.68 s; **2**, 2121.49 vs, 2107.18 s; **3**, 2122.02 vs, 2106.77 s; **4**, 2122.72 vs, 2105.83 s; **5**, 2123.57 vs, 2105.66 s; **6**, 2124.10 vs, 2105.57 s; **7**, 2124.59 vs, 2105.62 s; **8**, 2125.34 vs, 2105.42 s; **9**, 2125.79(8) vs, 2105.68(11) s; **10**, 2126.41 vs, 2105.64 s; **11**, 2124.55(5) vs, 2105.31(15) s; **12**, 2116.51 vs, 2106.97 s; **13**, 2117.55 vs, 2106.86 s; **14**, 2118.61 vs, 2107.16 s; **15**, 2119.48 vs, 2108.50 s. It should be noted that we do not imply accuracy of ± 0.01 cm^{-1} for these IR data. Conventionally these data would have been rounded to the ones place to match the resolution. However, the precision of these data is higher than the ones place as confirmed by the standard deviations. The average frequencies of three trials and standard deviations are reported for **9** and **11**. The non-rounded data form the trend discussed below, which could not be accurately expressed with rounded data.

Elemental Analysis. Elemental analyses were performed by Prevalere Life Sciences, Inc. (Whitesboro, NY), except for the analyses **3** and **13** which were performed at Galbraith Laboratories, Inc. (Knoxville, TN). **1**, $C_{24}H_{42}O_6N_{12}SmFe$, Calcd: C, 35.99; H, 5.29; N, 20.99. Found: C, 35.69; H, 5.07; N, 20.77. **3**, $C_{24}H_{42}O_6N_{12}GdFe$, Calcd: C, 35.69; H, 5.24; N, 20.81. Found: C, 35.43; H, 5.23; N, 20.69. **9**, $C_{24}H_{42}O_6N_{12}YbFe$, Calcd: C, 35.00; H, 5.14; N, 20.41. Found: C, 35.26; H, 4.73; N, 20.30. **13**, $C_{24}H_{42}O_6N_{12}CeFe$, Calcd: C, 36.46; H, 5.35; N, 21.26. Found: C, 36.26; H, 5.38; N, 20.97. **15**, $C_{24}H_{42}O_6N_{12}NdFe$, Calcd: C, 36.27; H, 5.33; N, 21.15. Found: C, 36.36; H, 5.22; N, 21.05 %.

X-ray Diffraction. Single crystals were filtered from the mother liquor and stored under N_2 until just before data collection. Data for **3**, **5**, **6**, **8**, **12**−**15** were collected on an Enraf-Nonius Kappa CCD diffraction system at 150 K (294 K for **6** and **8**), which employs a graphite monochromator with Mo K_α radiation (λ = 0.71073 Å). The crystals were mounted on the tip of glass fibers and coated with Fomblin oil (a perfluoropolyether). Unit cell parameters were obtained by indexing the first 10 frames and were refined employing the whole data set. All frames were integrated and corrected for Lorenz and polarization effects using DENZO-SMN package (Nonius BV, 1999).[21]

X-ray diffraction data for **1**, **4**, and **11** were collected on a Kappa goniostat with a SMART6000 CCD detector at ChemMatCARS (Advanced Photon Source, Argonne National Laboratory) at 95 K (273 K for **4** and **11**), which employs a diamond (111) monochromator with synchrotron radiation (**1**, λ = 0.43321 Å; **4** and **11**, λ = 0.49594 Å). X-ray diffraction data for **9** was collected on a Kappa goniostat with a Platinum 200 CCD detector at Beamline 11.3.1 (Advanced Light Source, Berkeley Lab) at 193 K, which employs a Channel-cut Si(111) monochromator with synchrotron radiation (λ = 0.77507 Å). The data frames for **1**, **4**, **11**, and **9** were processed using the SAINT program.[22]

Absorption corrections to data sets were carried out using the programs SCALEPACK (for **5**, **6**, **8**, **12**−**15**), SORTAV (for **3**) provided by MaXus software,[23] and SADABS[22] (for **1**, **4**, **11**, and **9**). All single crystal structures were solved using direct methods and refined using the SHELXTL-97 (difference electron density calculation, full matrix least-squares refinements).[24] After all non-hydrogen atoms were located and anisotropically refined, the hydrogen atoms of DMF were calculated assuming standard geometries. In compounds **12**−**15**, disordered carbon atoms of coordinated DMF solvent were isotropically refined. Data merging was performed for the data set of **3** using the data preparation program supplied by SHELXTL-97.

The recognition of disordered DMF methyl group carbon atoms (C13 of **12**; C13 of **13**; C42 and C62 of **14**; C33 and C53 of **15**) is based on SHELX97 which suggests that an atom with a U1 (the largest principal thermal ellipsoid axis) value greater than 0.2 Å and at least 2.5 times that of U2 (second largest thermal ellipsoid axis) is disordered. The disordered carbon atoms C61, C62, and C63 of **12**; C31, C32, and C33 of **14** represent two energetically similar conformations of DMF and were identified from the residual electron density peaks. All disordered carbon atoms were split, and the occupancies were estimated using PART 1 and PART 2 options in SHELX97.

X-ray powder diffraction data were collected on a Bruker D8 Advance X-ray powder diffractometer at room temperature (24(1) °C), which employs a Vario monochromator at the X-ray tube with Cu−$K_{\alpha 1}$ radiation (λ = 1.5406 Å). Samples were ground and sealed in 0.5 mm Lindeman glass capillaries loaded within the inert atmosphere drybox. The data were collected in 8 s steps of 0.0144° over the 2θ range 5−45°. The unit cell and atomic parameters obtained from the single crystal data were used as a starting point for the powder data refinement. The unit cell and experimental parameters (peak profile, scale, zero, background, March−Dollase[25] preferred orientation) were refined using GSAS[26] within EXPGUI.[27] The estimated error of each unit cell parameter, as calculated by GSAS, appeared to indicate unreasonably high accuracy. Therefore, three trials (X-ray powder diffraction and refinement) were performed for **1** to measure the actual error of each unit cell parameter. For each parameter of **1** in Table 1, the average of the three trials is reported along with its standard deviation.

(21) Otwinoski, Z.; Minor, W.; Processing of X-ray Diffraction Data Collected in Oscillation Mode. In *Methods in Enzymology, Vol. 276: Macromolecular Crystallography, Part A*; Carter, C. W., Jr., Sweet, R. M., Eds.; Academic Press: New York, 1997; pp 307−326.

(22) *SAINT v7.23A and SADABS v2.10 programs*; Bruker AXS, Inc.: Madison, WI, 2001.

(23) (a) Blessing, R. H. *Acta Crystallogr., Sect. A* **1995**, *51*, 33. (b) Blessing, R. H. *J. Appl. Crystallogr.* **1997**, *30*, 421. (c) Mackay, S.; Gilmore, C. J.; Edwards, C.; Tremayne, M.; Stuart, N.; Shankland, K. *MaXus: A Computer Program for the Solution and Refinement of Crystal Structures from Diffraction Data*; University of Glasgow: Scotland, Nonius BV: Delft, The Netherlands, and MacScience Co. Ltd.: Yokohama, Japan, 1998.

(24) Sheldrick, G. M. *SHELXTL-97: A Structure Solution and Refinement Program*; University of Göttingen: Göttingen, Germany, 1998.

(25) (a) March, A. *Z. Kristallogr.* **1932**, *81*, 285–297. (b) Dollase, W. A. *J. Appl. Crystallogr.* **1986**, *19*, 267–272.

(26) Larson, A. C.; Von Dreele, R. B. *GSAS (General Structure Analysis System): Los Alamos National Laboratory Report LUAR* **2000**, 86–748.

(27) Toby, B. H. EXPGUI: A graphical user interface for GSAS; *J. Appl. Crystallog.* **2001**, *34*, 210−213.

The standard deviations found for **1** were used as the estimated errors for **2**−**9**, **11**−**15**. Because of the absence of single crystal data for **2** and **7**, the powder data of **2** and **7** were refined using the atomic parameters (changing only the identity of the Ln atom: to Eu for **2**; to Er for **7**) from single crystal data of iso-structural compounds (**1**, **3**−**6**, **8**, **9**, and **11**) as the starting point. All eight refinements of **2** and **7** produced unit cell parameters that were the same within the estimated error.

Computational Methods. Although the explicit treatment of the 4f orbital of lanthanide complexes is still considerably challenging because of potential high spin configurations and considerable computational effort, it is believed generally that 4f electrons contribute little in the observed chemical behavior of many lanthanide complexes.[28] Therefore, it is possible to employ large core relativistic effective core potentials (RECP) optimized by the Stuttgart−Dresden group,[29,30] for which the 1s-4f shells are included in the core, to study the formal oxidation degree of the lanthanide (III) metals in $\{Ln^{III}(DMF)_6Fe^{III}(CN)_6\}$ complexes, while the 5s, 5p, 5d, and 6s electrons are explicitly considered in the valence shell. The corresponding 11-electron valence basis set was used for the trivalent lanthanide atom, and it was contracted as (7s6p5d)/[5s4p3d]. The Stuttgart-Dresden pseudopotential (ECP10MDF) was also employed for iron in combination with its corresponding optimized (8s7p6d2f1g)/[6s5p3d2f1g] basis set.[31,32] The cyanide group atoms were treated with the 6-31+G(d) basis set, while the DMF ligands were treated with the 3-21G basis set to reduce the computational demands.

Geometry optimizations were performed with C_i symmetry and followed by analytical computation of the second derivatives of the energy with regard to the nuclear coordinate to evaluate the vibrational frequencies for each structure. The predicted frequencies were not scaled. The B3PW91 density functional[33,34] which has yielded a good description for lanthanide complexes[28,35] at affordable computational effort was used to optimize the $\{Ln^{III}(DMF)_6Fe^{III}(CN)_6\}$ complexes for each Ln system. All of the calculations were carried out with the Gaussian 03 suite of programs at the Ohio Supercomputer Center.[36]

Magnetic Data. Magnetic susceptibility and magnetization measurements were carried out with a Quantum Design SQUID magnetometer MPMS-XL on crushed polycrystalline samples sealed in plastic bags in an inert atmosphere. Direct current (DC) magnetic measurements were performed with an applied field of 1000 Oe in the 1.8−300 K temperature range. Magnetization data were measured at 1.8 K with the magnetic field varying from 0 to 70000 Oe. The data were corrected for diamagnetic contributions by use of Pascal's constants.

Results and Discussion

Syntheses. It is impractical to prepare a water-free rare earth(III)-hexacyanoferrate(III) by a simple metathesis reaction between $K_3Fe(CN)_6$ and $LnCl_3$ in dry DMF because of the limited solubility of $K_3Fe(CN)_6$, $Ln(DMF)_6Fe(CN)_6$, and KCl (Reaction 1). When $K_3Fe(CN)_6$ and KCl form complexes with 18-Crown-6, the measured solubility values increase to 4.3 mmol/L and 260 mmol/L, respectively (see Supporting Information). The [(18-crown-6)K]Cl remained in solution when compounds **1**−**15** crystallized from dry DMF (Reactions 2 and 3).

$$LnCl_3 + K_3Fe(CN)_6 \xrightarrow{DMF} Ln(DMF)_6Fe(CN)_6\downarrow + 3KCl\downarrow \quad (1)$$

$$K_3Fe(CN)_6 + 3(18-Crown-6) \xrightarrow{DMF} [(18-Crown-6)K]_3Fe(CN)_6 \quad (2)$$

$$[(18-Crown-6)K]_3Fe(CN)_6 + LnCl_3 \xrightarrow{DMF} Ln(DMF)_6Fe(CN)_6\downarrow + 3[(18-Crown-6)K]Cl \quad (3)$$

The use of anhydrous reagents and dry DMF to obtain anhydrous solutions of $[(18\text{-crown-6})K]_3Fe(CN)_6$ or LnX_3 (Ln = rare earth element; X = Cl or NO_3) is the most straightforward approach (Reaction 2 and 3). However, Reaction 2 requires long reaction times with stirring and sonication. Furthermore, some anhydrous rare earth chlorides, such as $YbCl_3$, are slow to dissolve in dry DMF. Anhydrous rare earth nitrates are not commercially available for this method.

A better alternative requires the counterintuitive use of water to form the anhydrous solutions. Reaction 2 proceeds rapidly in water. Adding DMF and stirring under a dynamic vacuum at room temperature removes water and eventually leads to an anhydrous solution. The much lower vapor pressure of DMF compared to that of water aids this drying process. This method may also be applied to DMF solutions of $LnX_3 \cdot nH_2O$ (X = Cl, NO_3) which, under a dynamic vacuum, afford anhydrous DMF solutions of $LnX_3 \cdot n(DMF)$ (Reaction 4). The absence of an O−H stretching peak in the IR spectrum confirmed that the compound was anhydrous (see Supporting Information). Dry DMF is not required and air stable

(28) Maro, L.; Eisenstein, O. *J. Phys. Chem. A* **2000**, *104*, 7140.
(29) Dolg, M.; Stoll, H.; Savin, A.; Preuss, H. *Theor. Chim. Acta* **1989**, *75*, 173.
(30) Dolg, M.; Stoll, H.; Preuss, H. *Theor. Chim. Acta* **1993**, *85*, 441.
(31) Dolg, M.; Wedig, U.; Stoll, H.; Preuss, H. *J. Chem. Phys.* **1987**, *86*, 866.
(32) Martin, J. M. L.; Sundermann, A. *J. Chem. Phys.* **2001**, *114*, 3408.
(33) Becke, A. D. *J. Chem. Phys.* **1993**, *98*, 5648.
(34) Perdew, J. P.; Wang, Y. *Phys. Rev. B* **1992**, *45*, 13244.
(35) Wang, D.; Zhao, C.; Phillips, D. L. *Organometallics* **2004**, *23*, 1953.
(36) Frisch, M. J.; Trucks, G. W.; Schlegel, H. B.; Scuseria, G. E.; Robb, M. A.; Cheeseman, J. R.; Montgomery, J. A., Jr.; Vreven, T.; Kudin, K. N.; Burant, J. C.; Millam, J. M.; Iyengar, S. S.; Tomasi, J.; Barone, V.; Mennucci, B.; Cossi, M.; Scalmani, G.; Rega, N.; Petersson, G. A.; Nakatsuji, H.; Hada, M.; Ehara, M.; Toyota, K.; Fukuda, R.; Hasegawa, J.; Ishida, M.; Nakajima, T.; Honda, Y.; Kitao, O.; Nakai, H.; Klene, M.; Li, X.; Knox, J. E.; Hratchian, H. P.; Cross, J. B.; Bakken, V.; Adamo, C.; Jaramillo, J.; Gomperts, R.; Stratmann, R. E.; Yazyev, O.; Austin, A. J.; Cammi, R.; Pomelli, C.; Ochterski, J. W.; Ayala, P. Y.; Morokuma, K.; Voth, G. A.; Salvador, P.; Dannenberg, J. J.; Zakrzewski, V. G.; Dapprich, S.; Daniels, A. D.; Strain, M. C.; Farkas, O.; Malick, D. K.; Rabuck, A. D.; Raghavachari, K.; Foresman, J. B.; Ortiz, J. V.; Cui, Q.; Baboul, A. G.; Clifford, S.; Cioslowski, J.; Stefanov, B. B.; Liu, G.; Liashenko, A.; Piskorz, P.; Komaromi, I.; Martin, R. L.; Fox, D. J.; Keith, T.; Al-Laham, M. A.; Peng, C. Y.; Nanayakkara, A.; Challacombe, M.; Gill, P. M. W.; Johnson, B.; Chen, W.; Wong, M. W.; Gonzalez, C.; Pople, J. A. *Gaussian 03*, revision B.05; Gaussian, Inc.: Wallingford, CT, 2004.

Table 1. Crystallographic Information for **1**−**15**

	1		**2**	**3**		**4**	
empirical formula	$C_{24}H_{42}O_6N_{12}FeSm$		$C_{24}H_{42}O_6N_{12}FeEu$	$C_{24}H_{42}O_6N_{12}FeGd$		$C_{24}H_{42}O_6N_{12}FeTb$	
formula weight	800.90		802.48	807.80		809.47	
lattice	monoclinic		monoclinic	monoclinic		monoclinic	
space group	$C2/c$		$C2/c$	$C2/c$		$C2/c$	
Z	4		4	4		4	
XRD Method	single crystal	powder[h]	powder	single crystal	powder	single crystal	powder
a, (Å)	19.651(4)	19.86(3)	19.88(3)	19.732(4)	19.84(3)	19.654(4)	19.86(3)
b, (Å)	10.348(2)	10.40(2)	10.40(2)	10.343(2)	10.37(2)	10.327(2)	10.38(2)
c, (Å)	18.244(4)	18.33(3)	18.35(3)	18.202(4)	18.32(3)	18.146(4)	18.35(3)
β, (deg)	111.98(3)	112.56(2)	112.68(2)	112.13(2)	112.79(2)	112.14(2)	112.91(2)
volume, (Å^3)	3440.2(14)	3497(15)	3499(15)	3441.2(12)	3476(15)	3411.4(2)	3485(15)
D_{calc}, (g·cm^{-3})	1.546	1.520(6)	1.524	1.559	1.543	1.576	1.543
T, (°C)	−178(2)	24(1)	24(1)	−123(2)	24(1)	0(2)	24(1)
μ, (mm^{-1})	0.519[g]			2.386		0.979[i]	
R indices	R_1[a] = 0.0366	R_p[d] = 0.0162(24)	R_p[d] = 0.0168	R_1[a] = 0.0250	R_p[d] = 0.0206	R_1[a] = 0.0257	R_p[d] = 0.0139
	wR_2[b] = 0.1153	wR_p[e] = 0.0208(31)	wR_p[e] = 0.0216	wR_2[b] = 0.0477	wR_p[e] = 0.0258	wR_2[b] = 0.0698	wR_p[e] = 0.0176
	GOF[c] = 1.126	χ^{2f} = 1.757(284)	χ^{2f} = 1.770	GOF[c] = 1.049	χ^{2f} = 1.449	GOF[c] = 1.252	χ^{2f} = 1.876

	5		**6**		**7**	**8**	
empirical formula	$C_{24}H_{42}O_6N_{12}FeDy$		$C_{24}H_{42}O_6N_{12}FeHo$		$C_{24}H_{42}O_6N_{12}FeEr$	$C_{24}H_{42}O_6N_{12}FeTm$	
formula weight	813.05		815.48		817.77	819.48	
lattice	monoclinic		monoclinic		monoclinic	monoclinic	
space group	$C2/c$		$C2/c$		$C2/c$	$C2/c$	
Z	4		4		4	4	
XRD Method	single crystal	powder	single crystal	powder	powder	single crystal	powder
a, (Å)	19.692(4)	19.84(3)	19.866(4)	19.83(3)	19.81(3)	19.834(4)	19.80(3)
b, (Å)	10.319(2)	10.36(2)	10.375(2)	10.35(2)	10.34(2)	10.357(2)	10.35(2)
c, (Å)	18.177(4)	18.34(3)	18.368(4)	18.33(3)	18.33(3)	18.326(4)	18.32(3)
β, (deg)	112.33(3)	113.03(2)	113.13(3)	113.13(3)	113.21(2)	113.20(3)	113.28(2)
volume, (Å^3)	3416.5(14)	3468(15)	3481.5(15)	3462(15)	3452(15)	3460.1(15)	3447(15)
D_{calc}, (g·cm^{-3})	1.581	1.557	1.556	1.564	1.574	1.573	1.579
T, (°C)	−123(2)	24(1)	21(2)	24(1)	24(1)	21(2)	24(1)
μ, (mm^{-1})	2.649		2.725			3.020	
R indices	R_1[a] = 0.0256	R_p[d] = 0.0150	R_1[a] = 0.0272	R_p[d] = 0.0189	R_p[d] = 0.0173	R_1[a] = 0.0318	R_p[d] = 0.0174
	wR_2[b] = 0.0950	wR_p[e] = 0.0189	wR_2[b] = 0.0717	wR_p[e] = 0.0249	wR_p[e] = 0.0221	wR_2[b] = 0.0691	wR_p[e] = 0.0216
	GOF[c] = 1.172	χ^{2f} = 1.820	GOF[c] = 1.264	χ^{2f} = 2.898	χ^{2f} = 2.148	GOF[c] = 1.207	χ^{2f} = 2.445

	9		**11**		**12**	
empirical formula	$C_{24}H_{42}O_6N_{12}FeYb$		$C_{24}H_{42}O_6N_{12}FeY$		$C_{24}H_{42}O_6N_{12}FeLa$	
formula weight	823.59		739.46		789.46	
lattice	monoclinic		monoclinic		monoclinic	
space group	$C2/c$		$C2/c$		$P2/n$	
Z	4		4		4	
XRD Method	single crystal	powder	single crystal	powder	single crystal	powder
a, (Å)	19.768(4)	19.80(3)	19.639(4)	19.82(3)	19.303(4)	19.48(3)
b, (Å)	10.326(2)	10.34(2)	10.294(2)	10.35(2)	9.883(2)	10.01(2)
c, (Å)	18.258(4)	18.33(3)	18.150(4)	18.34(3)	19.550(4)	19.60(3)
β, (deg)	113.04(3)	113.36(2)	112.29(2)	113.06(2)	113.05(3)	113.47(2)
volume, (Å^3)	3429.6(14)	3444(15)	3395.0(2)	3460(15)	3431.7(14)	3507(15)
D_{calc}, (g·cm^{-3})	1.595	1.588	1.447	1.419	1.528	1.495
T, (°C)	20(2)	24(1)	0(2)	24(1)	−123(2)	24(1)
μ, (mm^{-1})	4.189[j]		0.859[i]		1.704	
R indices	R_1[a] = 0.0349	R_p[d] = 0.0110	R_1[a] = 0.0400	R_p[d] = 0.0176	R_1[a] = 0.0467	R_p[d] = 0.0182
	wR_2[b] = 0.0866	wR_p[e] = 0.0142	wR_2[b] = 0.1215	wR_p[e] = 0.0228	wR_2[b] = 0.1008	wR_p[e] = 0.1008
	GOF[c] = 1.047	χ^{2f} = 1.869	GOF[c] = 1.273	χ^{2f} = 2.635	GOF[c] = 1.046	χ^{2f} = 1.620

	13		**14**		**15**	
empirical formula	$C_{24}H_{42}O_6N_{12}FeCe$		$C_{24}H_{42}O_6N_{12}FePr$		$C_{24}H_{42}O_6N_{12}FeNd$	
formula weight	790.67		791.46		794.79	
lattice	monoclinic		monoclinic		monoclinic	
space group	$P2/n$		$P2/n$		$P2/n$	
Z	4		4		4	
XRD method	single crystal	powder	single crystal	powder	single crystal	powder
a, (Å)	19.385(4)	19.39(3)	19.292(4)	19.43(3)	19.349(4)	19.36(3)
b, (Å)	9.866(2)	9.98(2)	9.883(2)	10.00(2)	9.862(2)	9.97(2)
c, (Å)	19.434(4)	19.52(3)	19.486(4)	19.58(3)	19.410(4)	19.50(3)
β, (deg)	113.13(3)	113.60(2)	113.26(3)	113.73(2)	113.38(3)	113.86(2)
volume, (Å^3)	3418.0(14)	3461(15)	3413.2(14)	3483(15)	3399.7(14)	3442(15)
D_{calc}, (g·cm^{-3})	1.536	1.517	1.540	1.540	1.553	1.534
T, (°C)	−123(2)	24(1)	−123(2)	24(1)	−123(2)	24(1)

Table 1. Continued

	13		14		15	
μ, (mm^{-1})	1.793		1.889		1.991	
R indices	R_1[a] = 0.0413	R_p[d] = 0.0201	R_1[a] = 0.0403	R_p[d] = 0.0202	R_1[a] = 0.0307	R_p[d] = 0.0208
	wR_2[b] = 0.0847	wR_p[e] = 0.0257	wR_2[b] = 0.0981	wR_p[e] = 0.0259	wR_2[b] = 0.0652	wR_p[e] = 0.0267
	GOF[c] = 0.961	χ^{2f} = 1.398	GOF[c] = 1.111	χ^{2f} = 1.979	GOF[c] = 1.043	χ^{2f} = 1.479

[a] $R_1 = \sum||F_o| - |F_c||/\sum|F_o|$, for $I > 2\sigma(I)$. [b] $wR_2 = \{\sum w(F_o^2 - F_c^2)^2/\sum w(F_o^2)^2\}^{1/2}$, for all data. [c] $GOF = \sum w(|F_o| - |F_c|)^2/(N_{obs} - N_{var})$. [d] $R_p = \sum||I_o| - |I_c||/\sum|I_o|$. [e] $wR_p = \{\sum w(F_o^2 - F_c^2)^2/\sum w(F_o^2)^2\}^{1/2}$. [f] $\chi^2 = \sum w(I_o - I_c)^2/(N_{obs} - N_{var})$. [g] Value supplied by Advanced Photon Source, Argonne National Laboratory. [h] Average of three trials. [i] Calculated using Ag $K_{\beta 1}$ (μ/ρ) values.[31] [j] Value supplied by Advanced Light Source, Berkeley Lab.

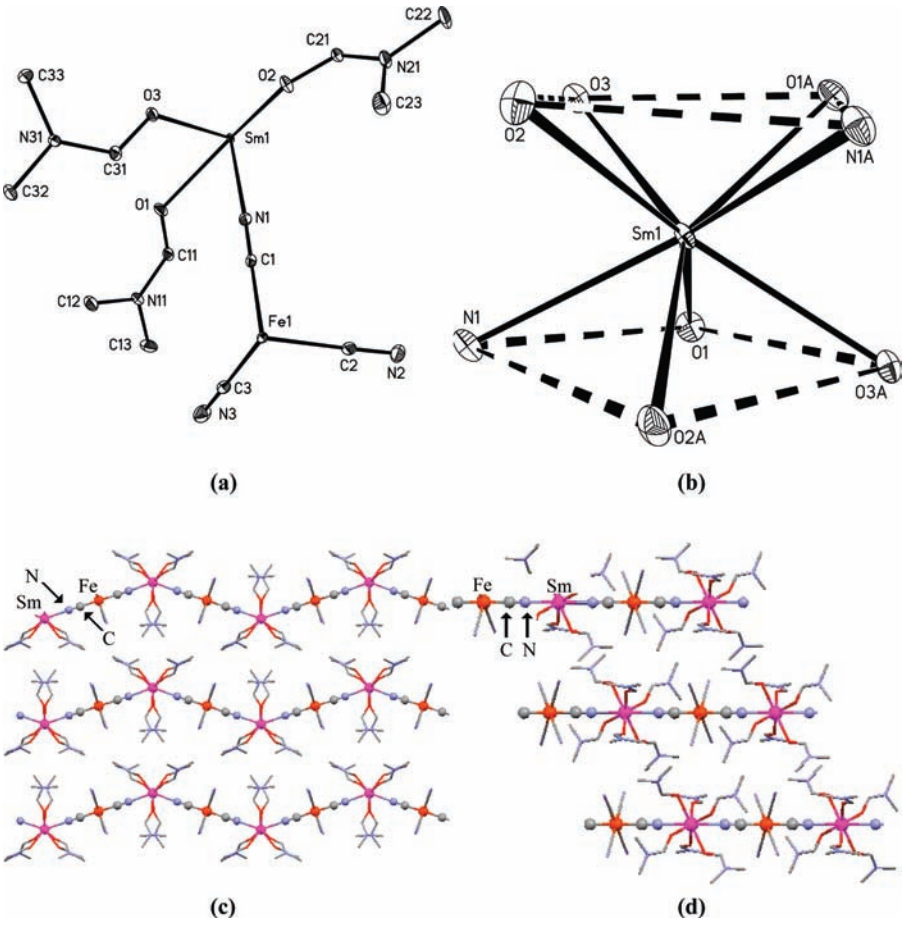

Figure 1. Crystal structure of $\{Sm(DMF)_6Fe(CN)_6\}_\infty$, **1**, with hydrogen atoms removed for clarity. (a) Asymmetric units (35% probability ellipsoids); (b) Coordination environment of Sm emphasizing the square antiprism geometry (35% probability ellipsoids); (c) Showing the zigzag shape of the linear chain fragment; (d) Showing the planar view of the linear chain fragment. This view is normal to that of (a) rotating about a horizontal axis.

reagents can be used. Evans et al. have demonstrated the preparation of anhydrous $Ln(NO_3)_3 \cdot n$(solvent) from $Ln(NO_3)_3 \cdot xH_2O$ using elevated temperatures with solvents of tetrahydrofuran and dimethoxyethane.[37]

$$LnCl_3 \xrightarrow{H_2O} LnCl_3 \cdot 6H_2O \xrightarrow[-H_2O]{DMF} LnCl_3 \cdot n\text{DMF} \quad (4)$$

Typical yields of **1**−**15** vary from 70−95%. Lower yields are likely due to mechanical loss rather than an incomplete reaction. When the yellow anion $[Fe(CN)_3]^{3-}$ is the limiting reagent, the reaction solution becomes colorless, implying complete consumption of the anion. Furthermore, some loss occurred during isolation because of the ease with which the product built up a static charge when removed from solvent, causing it to coat the glassware. Recrystallization of the water-free compounds was impractical. Despite their high solubility in water, **1**−**15** were insoluble in all other tested solvents.

Each of the two synthetic methods has advantages. The anhydrous route requires less solvent but requires dry solvent, a glove box, and a sonicator, while the other route requires much more solvent but does not require a drybox and sonicator

Crystal Structures. Crystallographic data for compounds **1**, **3**−**6**, **8**, **9**, and **11**−**15** are outlined in Table 1. These compounds form one-dimensional polymeric chains via isocyanide linkages (Figures 1 and 2). All lanthanide atoms are eight coordinate; six oxygen atoms and two nitrogen atoms are coordinated about the lanthanide atom in a distorted square-antiprismatic

(37) Evans, W. J.; Giarikos, D. G.; Workman, P. S.; Ziller, J. W. *Inorg. Chem.* **2004**, *43*, 5754–5760.

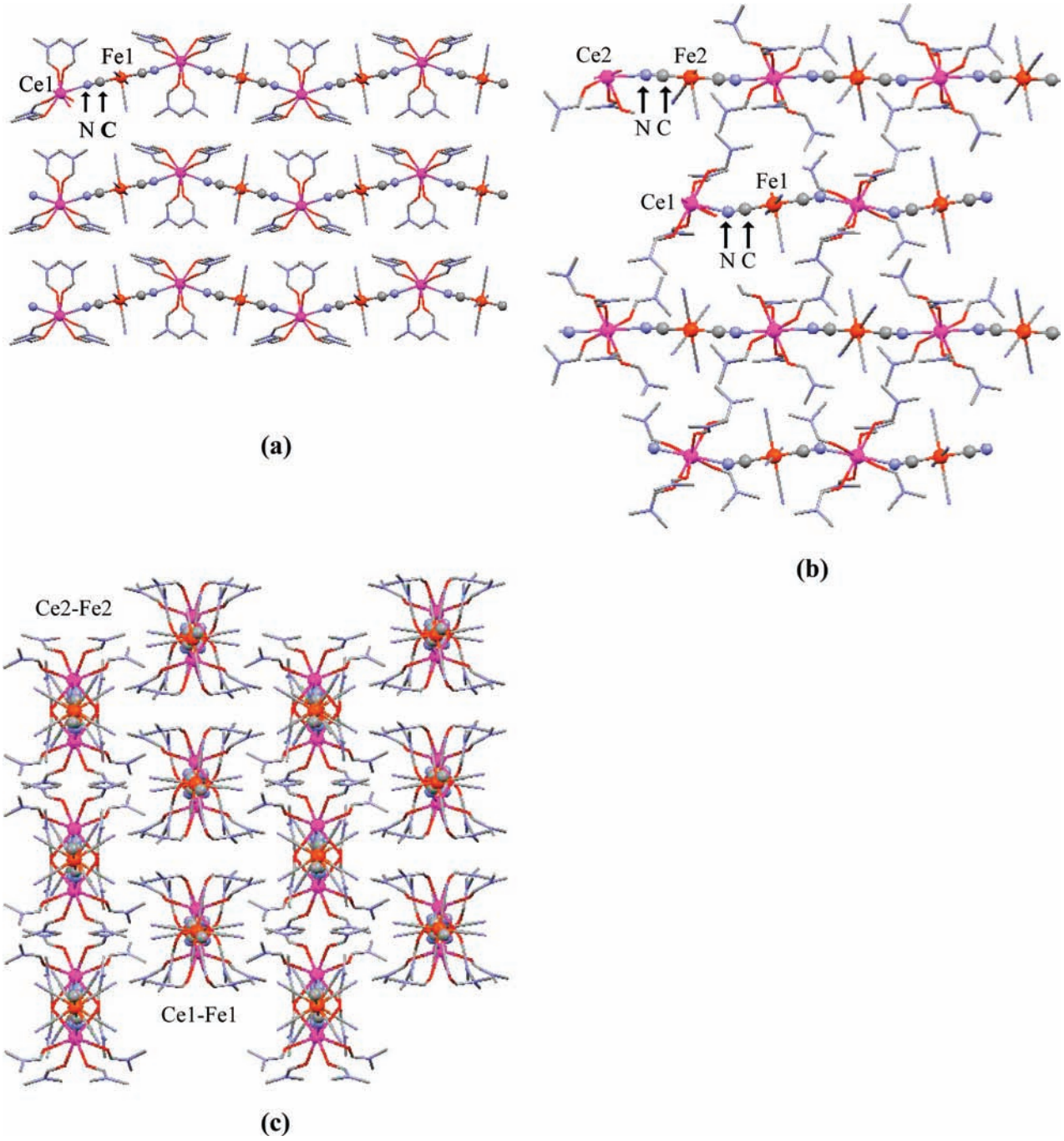

Figure 2. Extended crystal structure of $\{Ce(DMF)_6Fe(CN)_6\}_\infty$, **13**, with hydrogen atoms removed for clarity. (a) Showing the zigzag shape of the linear chain fragment containing Ce1 and Fe1; (b) Showing the planar view of the linear chain fragments. This view is normal to that of (a) rotating about a horizontal axis; (c) Looking down the extended polymeric chains. This view is normal to that of (a) rotating about the vertical axis.

geometry. Each iron atom is coordinated to six cyanide units. The octahedral geometry about the iron atom incorporates two bridging and four terminal cyanide units as *trans*-$[(\mu\text{-}CN)_2Fe(CN)_4]^{3-}$. No hydrogen bonding is observed. Two structural types have been observed for the series: space group $C2/c$ (structures **1**−**9**, and **11**) and space group $P2/n$ (structures **12**−**15**). Only structures of **1** (Figure 1) and **13** (Figure 2) are presented here to represent each structural morphology; however, structures **1**, **3**−**6**, **8**, **9**, and **11**−**15** are available in the Supporting Information. The $C2/c$ structure has one unique polymeric chain, while the $P2/n$ structure has two unique polymeric chains.

Figure 1a depicts the asymmetric unit of **1** while Figure 1b shows the coordination environment of the lanthanide cation. Distortion from the angles of an idealized square antiprism (70.5, 82.1, 109.5, 143.6°) is observed. Structures of **1**, **3**−**6**, **8**, **9**, and **11** have similar distortion patterns from these angles with the most pronounced distortion in N1−Ln1−O3A (**1**, 119.61(9); **3**, 119.72(7); **4**, 119.33(9); **5**, 119.69(10); **6**, 120.14(11); **8**, 120.08(20); **9**, 119.45(8); **11**, 119.43(8)°). The N1−Ln1−N1A angles for **1**, **3**−**6**, **8**, **9**, and **11** are (**1**, 140.99(10); **3**, 140.64(8); **4**, 141.10(10); **5**, 140.87(12); **6**, 140.67(12); **8**, 140.69(22); **9**, 140.95(9); **11**, 140.75(9)°) much larger than those observed in the one-dimensional compound of

Table 2. Selected Angles (deg) and Bond Lengths (Å) of **1**−**15** and Similar Compounds

compound	Ln−N−C	Ln−N	Ln−$O_{(DMF)}$	Ln−$O_{(H2O)}$	references
$Sm(H_2O)_2Fe(CN)_6\cdot 2H_2O$	166.4(7)	2.497(7)	none	2.404(7)	8b
	148.9(7)	2.532(7)			
$Sm(DMF)(H_2O)_3Fe(CN)_6\cdot H_2O$	170.2(5)	2.480(5)	2.330(4)	2.449(5)[b]	19
	168.2(5)	2.507(5)			
	148.7(5)	2.545(5)			
	153.9(5)	2.526(5)			
$Sm(DMF)_2(H_2O)_3Fe(CN)_6\cdot H_2O$	175.0(3)	2.513(3)	2.351(2)[a]	2.455(2)[b]	19
	165.3(3)	2.520(3)			
	152.2(3)	2.522(3)			
$Sm(DMF)_4(H_2O)_2Fe(CN)_6\cdot H_2O$	161.6(2)	2.543(3)	2.390(3)[a]	2.415(2)[a]	20
	158.0(2)	2.545(2)			
$Sm(DMF)_4(H_2O)_3Fe(CN)_6\cdot H_2O$	165.0(4)	2.505(5)	2.375(5)[a]	2.425(5)[b]	14
$Sm(DMF)_4(H_2O)_4Fe(CN)_6\cdot H_2O$	164.9(4)	2.504(4)	2.394(4)[a]	2.536(5)[b]	10
$Sm(DMF)_6Fe(CN)_6$, **1**	178.2(3)	2.525(3)	2.404(2)[a]	none	this work
$Gd(DMF)_6Fe(CN)_6$, **3**	177.5(2)	2.508(2)	2.374(2)[a]	none	this work
$Tb(DMF)_6Fe(CN)_6$, **4**	178.4(3)	2.495(3)	2.367(2)[a]	none	this work
$Dy(DMF)_6Fe(CN)_6$, **5**	178.0(3)	2.488(3)	2.354(3)[a]	none	this work
$Ho(DMF)_6Fe(CN)_6$, **6**	177.8(4)	2.483(4)	2.345(3)[a]	none	this work
$Tm(DMF)_6Fe(CN)_6$, **8**	177.5(6)	2.458(6)	2.329(5)[a]	none	this work
$Yb(DMF)_6Fe(CN)_6$, **9**	177.9(2)	2.447(3)	2.320(2)[a]	none	this work
$Y(DMF)_6Fe(CN)_6$, **11**	177.7(2)	2.477(2)	2.340(2)[a]	none	this work
$La(DMF)_6Fe(CN)_6$, **12**, La2	173.7(4)	2.664(4)	2.475(5)[a]	none	this work
$La(DMF)_6Fe(CN)_6$, **12**, La1	159.1(4)	2.580(5)	2.483(5)[a]		
$Ce(DMF)_6Fe(CN)_6$, **13**, Ce2	174.4(4)	2.630(4)	2.452(4)[a]	none	this work
$Ce(DMF)_6Fe(CN)_6$, **13**, Ce1	159.2(4)	2.560(4)	2.475(4)[a]		
$Pr(DMF)_6Fe(CN)_6$, **14**, Pr2	173.7(3)	2.626(3)	2.438(3)[a]	none	this work
$Pr(DMF)_6Fe(CN)_6$, **14**, Pr1	160.1(4)	2.541(4)	2.461(4)[a]		
$Nd(DMF)_6Fe(CN)_6$, **15**, Nd2	173.6(3)	2.598(3)	2.422(3)[a]	none	this work
$Nd(DMF)_6Fe(CN)_6$, **15**, Nd1	160.5(3)	2.526(3)	2.443(3)[a]		

[a] Averaged. [b] Averaged only coordinated H_2O.

$Sm(DMF)_4(H_2O)_2Fe(CN)_6$ (75.66(7)°)[20] which also contains distorted square-antiprismatic geometry about the lanthanide. For the structures of **1**, **3**−**6**, **8**, **9**, and **11**, the Ln−O, as well as the Ln−N, bond lengths become progressively shorter in accordance with the lanthanide contraction with values listed in Table 2.[38]

The extended structures of **1**, **3**−**6**, **8**, **9**, and **11** are one-dimensional polymeric chains as shown in Figure 1, panels c and d. The angles of Ln−N−C, listed in Table 2, are nearly linear. Figure 1c shows multiple linear fragments and emphasizes the zigzag arrangement due to the N1−Ln−N1A angle. In this figure, all Ln and Fe atoms are located in the same plane because of crystallographically imposed symmetry. Figure 1d shows the view normal to that of Figure 1c and emphasizes the planarity of the zigzag arrangement, as well as the arrangement of the polymeric chains. The Ln and Fe atoms are located at the Wyckoff sites 4*e* (2-fold rotational axis) and 4*c* (inversion center), respectively. Therefore, all Ln and Fe atoms of each polymeric chain are coplanar by crystallographic symmetry; however, the carbon and nitrogen atoms of bridging CN units are not coplanar. The N1−C1−Fe−C1A−N1A linear unit is angled slightly (**1**, 0.10(3); **3**, 0.37(2); **4**, 0.20(3); **5**, 0.33(3); **6**, 0.65(3); **8**, 0.65(5); **9**, 0.40(2), **11**, 0.23(2) °) about Fe1, from this plane. Six other chains surround each chain; Figure 1c depicts two of them. Figure 1d shows two chains (eclipsed) above and two chains (eclipsed) below. The chains are not stacked directly on top of each other.

The structures of **12**−**15** are similar. There are two unique eight coordinate Ln units (each similar to that shown in Figure 1b) that give rise to two unique polymeric chains in these structures as shown in Figure 2. One of the unique Ln centers (Ln2) gives rise to a planar zigzag polymeric chain, similar to those present in **1**−**9**, **11**. The other Ln center (Ln1) is part of a more distorted planar zigzag arrangement (Figure 2b). The pattern of distortion from the square antiprism is different between Ln1 and Ln2 but similar between the respective Ln units of **12**−**15**. The N−Ln1−N angles (**12**, 143.44(12); **13**, 144.34(18); **14**, 144.02(12); **15**, 144.00(14)°) are slightly larger than the N−Ln2−N angles (**12**, 141.03(12); **13**, 141.02(16); **14**, 141.21(12); **15**, 141.57(12)°). There is no notable difference between Ln1−O and Ln2−O bond lengths; however, the bond lengths of Ln2−N are longer than that of Ln1−N, as shown in Table 2. For the Ln−N−C angle, a very large difference is observed between Ln1 and Ln2. Ln2−N−C deviates from a linear arrangement only slightly, while the Ln1−N−C deviation is large. Furthermore, the view of Figure 2c shows that the Ln and Fe of each polymeric chain lie in the same plane. However, the bridging N−C−Fe−C−N unit within the fragment containing Ln1 has a larger angle from this plane (**12**, 9.75(3); **13**, 9.59(4); **14**, 9.36(3); **15**, 9.07(3)°) than the respective angle of Ln2 (**12**, 3.03(3); **13**, 2.87(3); **14**, 3.14(3); **15**, 3.06(3)°). The polymeric chain containing Ln1 repeats itself to form a plane of these chains as shown in Figure 2b. An arrangement of linear fragments containing Ln2 forms a similar plane. These two planes are alternately stacked on top of one another.

(38) (a) Huheey, J. E.; Keiter, E. A.; Keiter, R. L. *Inorganic Chemistry Principles of Structure and Reactivity*, 4th ed.; Harper Collins College Publishers: New York, 1993.(b) Vegard, L.; Dale, H. Z. Kristallogr. 1928, 67, 148. (c) Hazen, R. M; Finger, L. W. Comparative Crystal Chemistry; Wiley: New York, 1982.(d) Pearson, W. B. The Crystal Chemistry and Physics of Metals and Alloys; Wiley: New York, 1972.

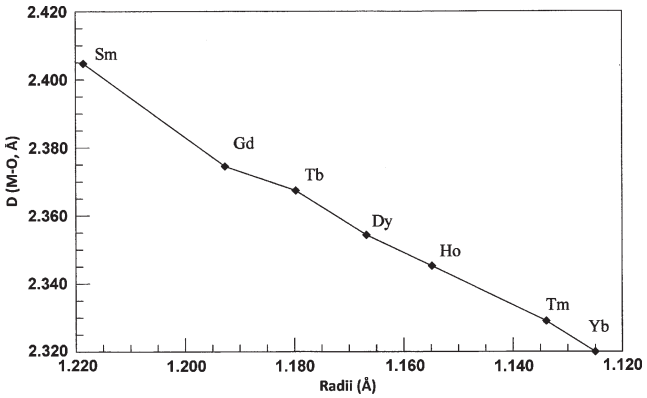

Figure 3. Lanthanide Contraction, a plot of the lanthanide-oxygen distances versus the empirical lanthanide radii.[38a]

In compounds **1**, **3**−**6**, **8**, **9**, and **11**−**15**, the C−N bond lengths range from 1.165(8) to 1.139(9) Å without a noticeable trend. In structures **1**, **3**−**6**, **8**, **9**, and **11**, the Fe−$C_{(\mu\text{-CN})}$ bond length (**1**, 1.922(3); **3**, 1.933(3); **4**, 1.925(3); **5**, 1.929(3); **6**, 1.931(4); **8**, 1.927(6); **9**, 1.936(3); 11, 1.929(3) Å) is shorter than Fe−$C_{(\text{terminal-CN})}$ bond lengths (**1**, 1.957(4), 1.961(4); **3**, 1.959(3), 1.962(3); **4**, 1.950(4), 1.954(4); **5**, 1.952(5), 1.957(5); **6**, 1.957(6), 1.957(6); **8**, 1.961(11), 1.966(10); **9**, 1.954(4), 1.959(4); 11, 1.961(4), 1.954(3) Å). In structures **12**−**15**, two unique Fe centers are present, and each center also exhibits a shorter Fe−$C_{(\mu\text{-CN})}$ than Fe−$C_{(\text{terminal-CN})}$ bond length; however, one of the Fe centers (Fe2) has a more subtle distinction between the bridging and terminal bond lengths (Fe−$C_{(\mu\text{-CN})}$: **12**, 1.924(6), 1.942(5); **13**, 1.929(5), 1.947(5); **14**, 1.921(5), 1.947(3); **15**, 1.927(4), 1.946(4); Fe−$C_{(\text{terminal-CN})}$: **12**, 1.955(8), 1.960(6), 1.952(6), 1.956(5); 13, 1.946(7), 1.958(6), 1.952(6), 1.956(6); **14**, 1.952(7), 1.954(7), 1.955(5), 1.961(6); **15**, 1.954(5), 1.955(5), 1.964(4), 1.960(4) Å).

Formation of the different structures can be attributed to the larger Ln radius of **12**−**15** compared to those of **1**−**9**, and **11**. As seen in our previous studies[39] of $(DMF)_xLn_2[M(CN)_4]_3$ (Ln = rare earth elements; M = Ni, Pd, Pt; x = 10, 12), different structure types are displayed for the larger and smaller rare earth elements. The most distinct difference is the coordination number of the rare earth elements, being 9-coordinate for larger elements and 8-coordinate for the smaller elements. However, in compounds **1**−**9** and **11**−**15**, the coordination number remains unchanged. Two structure types are observed. With the larger size and coordination space about the Ln, the $[Fe(CN)_6]^{3-}$ anion approaches the lanthanide at an angle (Ln−N−C angle < 180°), allowing a closer interaction with the anion. This interaction may be preferred over the coordination of an additional DMF molecule because of the elevated anionic charge and steric demands of $[Fe(CN)_6]^{3-}$ in comparison to $[M(CN)_4]^{2-}$. The distance between Ln1 and Fe1 (**12**, 5.557(2); **13**, 5.537 (2); **14**, 5.521(2); **15**, 5.512(2) Å) is shorter than that of the Ln2 and Fe2 (**12**, 5.744(2); **13**, 5.725(2); **14**, 5.709(2); **15**, 5.689(2) Å) while *C*2/*c* structures give intermediate Ln−Fe distances (**1**, 5.598(2); **3**, 5.593(1); **4**, 5.574(2); **5**, 5.569(2); **6**, 5.565(2); **8**, 5.549(2); **9**, 5.541(2); **11**, 5.561(2) Å).

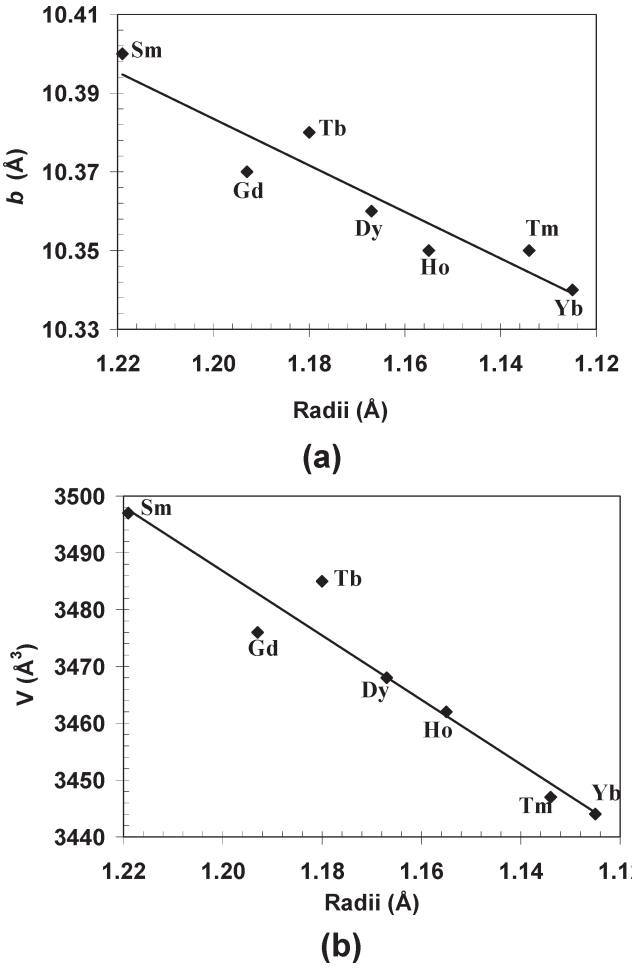

Figure 4. Failure of " Vegard's Rule". (a) Plot of cell constant B versus empirical lanthanide radii.[38a] (b) Plot of cell volume versus empirical lanthanide radii.[38a]

Structural Considerations. Structural evidence for the Lanthanide Contraction is given in Figure 3.

The applicability of "Vegard's Rule"[38b] to structural information obtained in this investigation was examined. Essentially, this "rule" predicts a linear relationship between some unit cell parameter such as cell volume or a cell axis versus the size of an ion in the structure for an isomorphic series of structures. While "Vegard's Rule"[38b] has been shown to apply for rigid ionic crystals,[38c] it is less successful for application to alloys[38d] and in systems that consist of complex molecules of flexible structure. Figure 4 shows an approximate linear relationship for a monotonic increase in unit cell volume or cell constant with the systematic increase in ionic radius of atoms substituted in the isomorphic series of compounds **1**, **3**−**6**, **8**, **9**, consistent with "Vegard's Rule". Data for Figure 4 were taken from X-ray powder results given in Table 1. All of the data were obtained at 24 °C. Single crystal data were not employed in these plots because all the X-ray data were not collected at the same temperature.

IR Spectra. The IR spectra of **1**−**15** contain only absorptions associated with DMF and cyanide ligands.

(39) (a) Liu, J.; Knoeppel, D. W.; Liu, S.; Meyers, E. A.; Shore, S. G. *Inorg. Chem.* **2001**, *40*, 2842–2850. (b) Plečnik, C. E.; Liu, S.; Shore, S. G. *Acc. Chem. Res.* **2003**, *36*, 499–508. (c) Knoeppel, D. W.; Liu, J.; Meyers, E. A.; Shore, S. G. *Inorg. Chem.* **1998**, *37*, 4828–4837. (d) Du, B.; Ding, E.; Meyers, E. A.; Shore, S. G. *Inorg. Chem.* **2001**, *40*, 3637–3638. (e) Knoeppel, D. W.; Shore, S. G. *Inorg. Chem. Commun.* **1996**, *35*, 1747–1748.

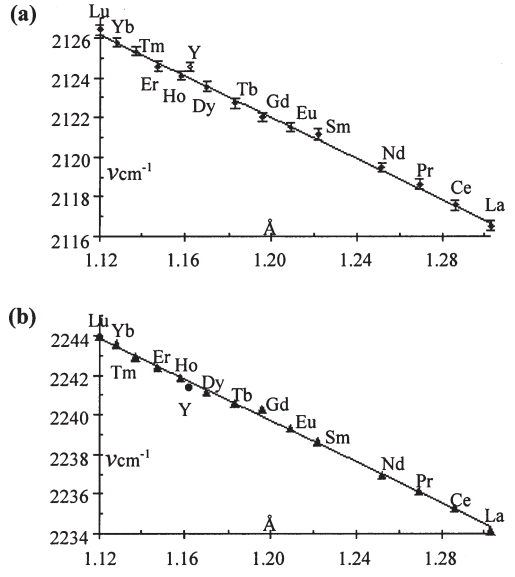

Figure 5. Plot of 8-coordinate Ln^{3+} ionic radius (x)[38] versus stretching frequency (y) of the bridging CN mode. (a) Experimental data of **1**−**10**, **12**−**15**, have a calculated linear regression ($y = -51.495x + 2183.7$; $R^2 = 0.9961$). (b) Analogous computational data of **1**−**10**, **12**−**15**, have a calculated linear regression ($y = -52.471x + 2302.5$; $R^2 = 0.9984$).

No peaks were observed above 3150 cm^{-1}, thus confirming water-free syntheses. Each compound exhibits two major absorptions in the CN stretching region representing μ-CN and, at a lower frequency, terminal CN. The $\nu_{\mu\text{-CN}}$ absorptions of compounds **1**−**10**, **12**−**15** exhibit a linear relationship with the 8-coordinate Ln^{3+} ionic radius (Figure 3a). The estimated error of $\nu_{\mu\text{-CN}}$ of **9** is three times the standard deviation ($3\sigma = 0.25\ cm^{-1}$). The error bars used in Figure 5a for compounds **1**−**10**, **12**−**15** are $\pm 0.25\ cm^{-1}$. The Lewis acidity of the Ln^{3+} metal seems to be the best explanation of the ionic radius-$\nu_{\mu\text{-CN}}$ relationship,[3] and the precision of the IR data has allowed for the identification of this relationship. If the data were rounded off in the name of accuracy, the deviation of **11** from the relationship would not have been identified. Three trials of **11** confirm that it deviates slightly from the $\nu_{\mu\text{-CN}}$-radius relationship. The lighter mass of yttrium compared to other Ln metals in the series could explain, by the kinematic effect, a deviation lower than the series **1**−**10**, **12**−**15**.[3] However, a deviation higher than the series is observed, and this could be explained by a better orbital overlap of the empty 4d orbitals of Y^{3+} with the anti-bonding nitrogen lone pair compared to empty of 5d (or 4f) of the Ln^{3+} series. The estimated error and the error bars used in Figure 5a for **11** are three times the standard deviation ($3\sigma = 0.16\ cm^{-1}$).

Computational Analysis. For comparison with the single crystal structure, the fully optimized computational model (shown in Figure 6) of **1** has an average Sm^{3+}−O bond length of 2.424 Å, which is only 0.02 Å longer than the single crystal data. The Sm^{3+}−N1 bond length is also in agreement with the single crystal data (2.546 Å vs 2.525(3) Å). These values, along with the other parameters, confirm that the calculated geometric model is consistent with the crystal structure of **1**. The other single crystal structures also demonstrate this consistency with the computational models. The computational results confirm that both Ln^{3+}−O and Ln^{3+}−N1 bond length

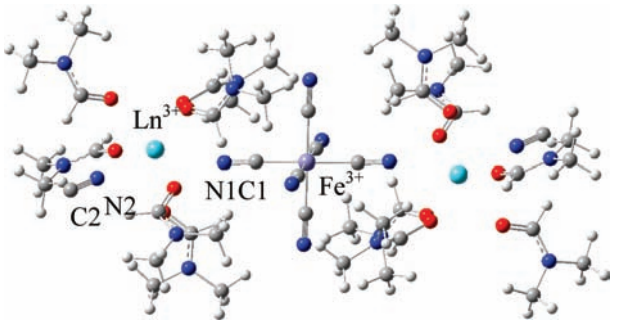

Figure 6. Computational model ($[CNLn(DMF)_6]_2Fe(CN)_6$) and atomic labels are referred to within the discussion. This model has C_i symmetry with iron at the inversion center. The colors represent the following atoms: gray, carbon; white, hydrogen; red, oxygen; blue, nitrogen.

averages increase in a monotonic manner with respect to the Ln^{3+} ionic radii (see Supporting Information).

The predicted $\nu_{\mu\text{-CN}}$ frequencies (C1N1 in Figure 6) exhibit a linear relationship with the 8-coordinate Ln^{3+} ionic radius (Figure 5b), which is consistent with the experimental data of **1**−**10**, **12**−**15**. While the non-scaled computational $\nu_{\mu\text{-CN}}$ data are not identical to experimental $\nu_{\mu\text{-CN}}$ data, the correlation of the vibrational frequencies with the Ln^{3+} ionic radius are very similar, the total range of vibrational frequencies is similar (~10 cm^{-1}), and the trends also yield similar slopes (theory, −52.3, versus expt, −51.5) for the dependence of the CN stretching frequency on the Ln's ionic radius. The computational studies imply that the 4f electrons of Ln^{3+} play little role in this linear trend since the 4f electrons of Ln^{3+} were treated in the large core RECP.

X-ray Powder Diffraction. While elemental analyses confirm the empirical formula $C_{24}H_{42}O_6N_{12}LnFe$, and confirm that the bulk sample is chemically consistent with the single crystal X-ray structures, they do not resolve the question that these compounds might crystallize as mixtures of two different crystalline phases with the same chemical composition. In the present study, this was a real consideration since single crystal X-ray analyses identified **1**−**9** and **11** as crystallizing in the $C2/c$ space group while **12**−**15** crystallize in the $P2/n$ space group. Possibly, a second crystalline phase coexisted with those observed but was not recognized because a single crystal of this second phase in the mixture could not be obtained. X-ray powder diffraction results confirm that the bulk crystalline samples are structurally homogeneous and consistent with the single crystal X-ray structures. Cell parameters are in agreement with those obtained from single crystal X-ray data (Table 1). No unexplained reflections were observed in the powder data. A typical observed pattern with respect to the pattern calculated from the single crystal structure is shown in Figure 7.

Static Magnetic Properties. Magnetic susceptibility measurements for compounds **3**−**6**, **8**, **11** were performed on polycrystalline samples of the compounds at 1000 Oe over the temperature range 1.8−300 K by using a SQUID magnetometer. The model compound **11** with diamagnetic Y^{III} ions serves to determine the magnetic behavior of the low-spin Fe(III) ion. The room-temperature χT value of **11** is 0.61 emu·mol^{-1}·K, which is close to the expected diamagnetic Y^{III} ion ($\chi T = 0.00$ emu·mol^{-1}·K)

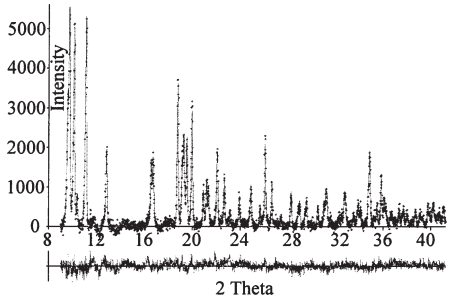

Figure 7. Background corrected X-ray powder diffraction data of Sm $(DMF)_6Fe(CN)_6$, **1**, is displayed as points. The calculated powder pattern as determined by refinement using GSAS is depicted as a solid line. At the bottom of the figure, a solid line depicts the difference plot (calculated − observed).

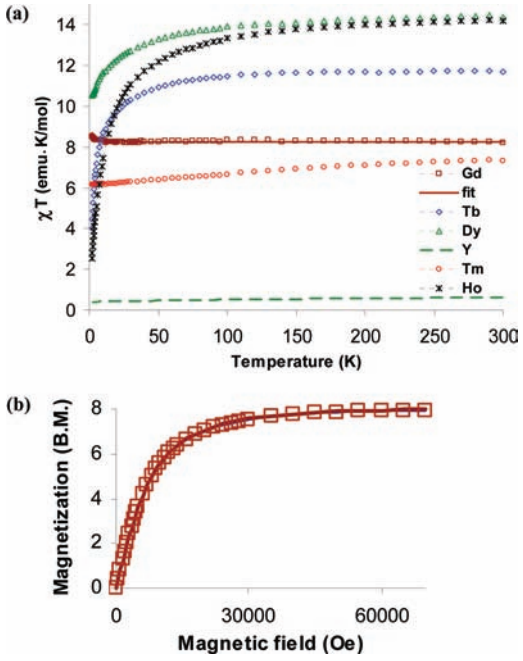

Figure 8. (a) Temperature dependence of the χT product for **3**−**6**, **8**, **11**. (b): The field dependent magnetization of the **3** at 1.8 K, in the range of 0−7 T.

and the low-spin Fe(III) ion ($S = 1/2$, $g = 2.1$) with an orbital contribution.[40] The value continuously decreases from the value at room temperature and reaches a minimum of 0.42 emu·mol^{-1}·K at 2 K, (Figure 8). The room temperature χT values for **4**−**6** and **8** are close to the theoretical ones for the superposition of isolated Ln(III) and low-spin Fe(III) ions, namely 11.68, 14.38, 14.17, and 7.33 emu mol^{-1} K, respectively (Figure 8). The χT values decrease smoothly with decreasing temperature, because of the depopulation of excited Stark sublevels, reaching values of 4.46, 10.5, 2.8, and 6.15 emu mol^{-1} K at 2 K for compounds **4**−**6** and **8**, respectively. No significant magnetic interactions were observed for these compounds. The room-temperature χT value of **3** is 8.25 emu·mol^{-1}·K, which is the expected value for a spin-only case of an uncoupled Gd(III) ion ($^8S_{7/2}$ ground state, χT = 7.88 emu·mol^{-1}·K) and low-spin Fe(III) ion. The value is nearly over the entire temperature range. Below 8 K, the χT value slightly increases to reach a maximum of 8.68 emu·mol^{-1}·K at 2 K. The temperature dependence of $1/\chi$ approximates Curie−Weiss behavior with $C = 8.25$ emu·mol^{-1}·K and $\theta = 0.1$ K. The small positive Curie−Weiss constant may indicate a slight ferromagnetic coupling between Gd(III) and Fe(III) ions. The field-dependent isothermal magnetization, $M(H)$ at 1.8 K fits well to the superposition of the two Brillouin functions calculated for Fe(III), $S = 1/2$, $g = 2.0$ and Gd (III), $S = 7/2$, $g = 2.0$ (Figure 8b).

Summary. The syntheses reported here for **1**−**15** are the first of a water-free DMF solvated rare earth−hexacyanoferrate(III). All structures contain 8-coordinate Ln(III) metal centers with nearly identical coordination environments. Powder X-ray diffraction results were employed as the primary method for bulk sample confirmation. For compounds **1**−**15**, powder X-ray diffraction results were more informative than elemental analysis data, which were difficult to obtain. Infrared data reveal a linear relationship between the ionic radius of the lanthanide and the $\nu_{\mu\text{-CN}}$ stretching frequency, while Y deviates slightly from this relationship.

Magnetic susceptibility measurements for compounds **3**−**6**, **8**, **11** were performed on polycrystalline samples of the compounds.

Acknowledgment. This work was supported by the National Science Foundation through Grant CHE 02-13491. Maren Pink contributed to the single crystal X-ray data collection of **1**, **4**, and **11** while Jeanette Krause collected that of **9**. ChemMatCARS Sector 15 is principally supported by the National Science Foundation/Department of Energy under Grant CHE-0535644. Use of the Advanced Photon Source was supported by the U. S. Department of Energy, Office of Science, Office of Basic Energy Sciences, under Contract No. DE-AC02-06CH11357. Christopher M. Potratz collected the single crystal X-ray data sets for **12** and **14**. Michelle Doglos and Patrick M. Woodward have given much advice pertaining to powder X-ray diffraction. The Ohio Supercomputer Center (OSC) is acknowledged for generous computational support of this research.

Supporting Information Available: Supplementary molecular structures, solid-state IR spectra, atomic coordinates used for computational analysis, calculated IR frequencies, and X-ray crystallographic files in CIF format of the compounds. This material is available free of charge via the Internet at http://pubs.acs.org.

(40) Zhao, H.; Lopez, N.; Prosvirin, A.; Chifotides, H.; Dunbar, K. *Dalton Trans.* **2007**, 878–888.